The Regional Diagnosis of Onset and Demise of the Rainy Season over Tropical and Subtropical Australia

VASUBANDHU MISRA,[a,b,c] SHUBHAM DIXIT,[d,c,b] AND C. B. JAYASANKAR[b,c]

[a] *Department of Earth, Ocean and Atmospheric Science, Florida State University, Tallahassee, Florida*
[b] *Center for Ocean–Atmospheric Prediction Studies, Florida State University, Tallahassee, Florida*
[c] *Florida Climate Institute, Florida State University, Tallahassee, Florida*
[d] *Rickards High School, Tallahassee, Florida*

(Manuscript received 19 October 2022, in final form 6 March 2023, accepted 8 March 2023)

ABSTRACT: In this paper, we introduce a novel strategy to robustly diagnose the onset and demise of the rainy season using daily observed rainfall over seven specific regions across Australia, as demarcated by the Natural Resource Management (NRM) agency of Australia. The methodology lies in developing an ensemble spread of the diagnosed onset and demise from randomly perturbing the observed daily time series of rainfall at synoptic scales to obtain a measure of the uncertainty of the diagnosis. Our results indicate that the spread of the ensemble in the diagnosis of the onset and demise dates of the rainy season is higher in the subtropical region than the tropical region. Secular change of earlier onset, later demise, longer length, and wetter season are also identified in many of these regions. The influence of the PDO at decadal scale, ENSO and Indian Ocean dipole at interannual scale, and MJO at intraseasonal scale also reveals significant influence on the evolution of the rainy season over these regions in Australia. Most important, the covariability of the onset date with the length of the season and seasonal rainfall anomaly of the season is highlighted as a valuable relationship that can be exploited for real-time monitoring and providing an outlook of the forthcoming rainy season, which could serve some of the NRM regions.

SIGNIFICANCE STATEMENT: We document the rainfall variability during the rainy season over tropical, subtropical, and semiarid regions of Australia and relate them to modes of climate variability spanning from intraseasonal to secular time scales. The study highlights the varied influence of the modes of climate variability on various aspects of the evolution of the rainy season, such as its onset and demise dates and the seasonal rainfall anomaly over these Australian regions. The study uses 114 years of data and shows that the variations in the length of the rainy season and its seasonal rainfall anomaly are strongly dictated by variations of rainy-season onset date. This provides a quick seasonal outlook of the forthcoming rainy season by just monitoring the onset-date evolution in these regions.

KEYWORDS: Climate; Climate variability; ENSO; Hydrometeorology

1. Introduction

Northern Australia is well known for its distinct rainy season (Nicholls et al. 1982; Nicholls 1984; Lo et al. 2007; Lisonbee et al. 2020; Uehling and Misra 2020, hereinafter UM20; Uehling et al. 2021, hereinafter U21). The variability of the onset, demise, and intensity of the Australian monsoon season is of great significance to those who depend on the seasonality of the rainy season (e.g., practitioners in water and energy sectors, agriculturists, and graziers). As noted in Lisonbee et al. (2020) and U21, the definition of the rainy or the wet season in Australia is varied. In many instances, the seasons are fixed to calendar months [e.g., Lo et al. (2007) and the Bureau of Meteorology (2023) recognize October to the following April as the wet season of northern Australia, north of 26°S]. Alternatively, other studies associate the rainy season with the shift of the monsoonal low-level winds (e.g., Troup 1961; Holland 1986). In this study, as in UM20 and U21, the rainy season is defined by the first day of the year when the rain rate exceeds the annual mean climatology and ends on the first day of the following year when the rain rate falls below the annual mean climatology for the location. This definition of the rainy season normally tends to commence earlier, before the onset, and extends after the demise of the monsoon season (Nicholls et al. 1982; UM20; U21). In UM20, U21, and this study, the onset and demise of the rainy season are based purely on the seasonal cycle of rainfall and do not consider the seasonal cycle of other upper-air variables (e.g., circulation fields). In UM20, the onset and demise of the rainy season were diagnosed for the aggregate continental region of northern Australia (north of 20°S). In U21, the onset and demise of the rainy season were calculated at each grid point of the gridded rainfall dataset to provide an understanding of the local variations and spatial heterogeneity. In this study, we have adapted the diagnosis of the onset and demise of the rainy season based on Natural Resource Management (NRM) agency subclusters (https://www.climatechangeinaustralia.gov.au/en/overview/impacts-and-adaptation/nrm-regions/; Fig. 1).

Corresponding author: Vasubandhu Misra, vmisra@fsu.edu

Earth Interactions is published jointly by the American Meteorological Society, the American Geophysical Union, and the Association of American Geographers.

DOI: 10.1175/EI-D-22-0026.1 e220026

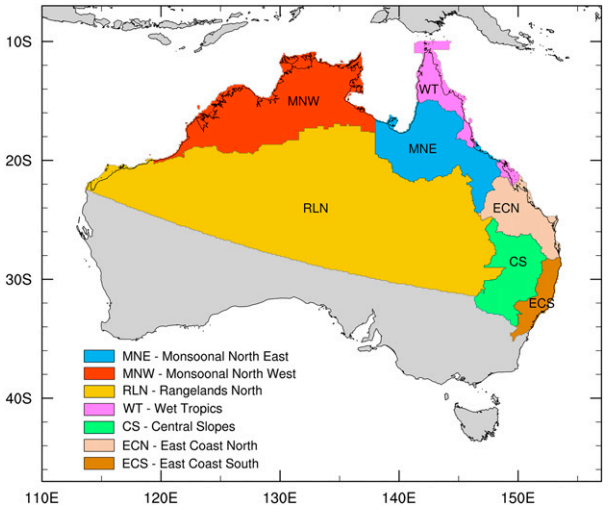

FIG. 1. The seven regions for which the analysis of their rainy season is conducted in this study.

The NRM clusters are based on broadscale climate and biophysical regions of Australia. To sustain the country's unique and diverse natural resources, these clusters are in focus to develop a response to potential impacts of climate change. Many of these clusters (Fig. 1) have been further subdivided into subclusters [e.g., monsoonal north to monsoonal northwest (MNW) and monsoonal northeast (MNE); east coast to east coast north (ECN) and east coast south (ECS); rangelands to rangeland north (RLN) and rangeland south (RLS; not shown in Fig. 1)] to provide a more refined level of climate projection. We have adopted many of these subclusters in our present study that are known to display a very strong seasonal cycle of rainfall that is associated and nearly coincident with the Australian monsoonal season. In relation to UM20 and UM21, this study offers several variations, including the change in the granularity of the analysis, inclusion of a perturbation method to assess the uncertainty in the diagnosis of the onset and demise dates of the rainy season, and the relation of their variations to several modes of climate variability spanning from the intraseasonal to the secular time scales. The granularity of the analysis has a significant bearing on the interpretation of the results because the associated NRM activity is dependent on the scale of the climate analysis (Bardsley and Rogers 2010; Adams et al. 2017). For example, Cowan et al. (2020) provide a motivation for their study by suggesting that forecast products from the Bureau of Meteorology targeted to graziers of northern Australia do not exist, who critically depend on the onset of the rainy season. On the other hand, they indicate that there are specific forecast products for southern Australian horticultural regions, management of the Great Barrier Reef to the east, and fisheries, that are significantly used by the stakeholders. Likewise, the subclusters in Fig. 1 support varied land-use activities (e.g., agriculture, forestry, nature conservation, pastoralism, oil and gas exploration, mining, tourism), which demand subcluster-specific climate information that this paper is attempting to target. Additionally, contrasting the variability of the rainy seasons in these regions will provide a perspective on the relative challenges of anticipating these variations and developing appropriate adaptation plans to mitigate impacts.

There has been considerable work related to the variability of the Australian monsoon from intraseasonal scales (e.g., Holland 1986; Hendon and Liebmann 1990; Evans et al. 2014), interannual scales (e.g., McBride and Nicholls 1983; Kajikawa et al. 2010; Catto et al. 2012) to decadal scales (e.g., Power et al. 1999; Meehl and Arblaster 2011; Heidemann et al. 2022), and secular time scales (Hennessey et al. 1999; Taschetto and England 2009; Freund et al. 2017). Hence, this study spans these variations for the rainy season over the specific subclustered regions of Australia shown in Fig. 1.

In this study we also introduce an ensemble approach to the diagnosis of the observed variations of the rainy season in these subclusters of tropical, semiarid, and subtropical Australia that provides a measure of the uncertainty of the results. The accounting of the uncertainty of the rainfall data is very important given the objectivity and the preciseness of the diagnosis of the onset and demise of the rainy season. However, even rain gauge–based observations like the one used in this study, following Grant (2012), are susceptible to observational errors (Jones et al. 2009). For example, Jones et al. (2009) find that the number of rain gauge stations reporting daily in Australia increased from around 3200 in 1900 to around 6500 around 2010. Furthermore, the distribution of the rain gauge station network across Australia is uneven, with eastern and southwestern Australia having the densest coverage in comparison with central Australia and parts of northern Australia (Jones et al. 2009). Furthermore, the errors of the rain gauge measurements are a cause of observational rainfall uncertainty (Adam and Lettenmaier 2003; Sevruk et al. 2009; Schneider et al. 2014). Ehsani and Behrangi (2022) suggest that the systematic errors in rain gauge measurements essentially arise from influence of winds and evaporation losses, leading to undercatch. Finally, the definition of the onset and demise of the rainy season adopted in this study hinges on the seasonal cycle of rainfall; therefore, the uncertainty of its diagnosis from synoptic variations of rainfall needs to be assessed.

2. Datasets and methodology

In this study, we make use of the Australian Bureau of Meteorology's rain gauge analysis available across the Australian continent (Grant 2012). The daily dataset is available on a $0.05° \times 0.05°$ grid from January 1900 to 31 December 2015. Like any other gridded dataset, the underestimation of peak values reported at stations and inevitable smoothing of data are some of the immediate limitations of this rainfall dataset (King et al. 2013; Evans et al. 2020). The Bureau's rainfall analysis is an outcome of a rigorous quality control on the station data and is done in several layered approaches, including manual, automated quality control procedures, and an integrated cross-validation procedure before the final analysis is produced (Evans et al. 2020). It is further reported that for much of Australia, the fractional area that contains at least one monthly reporting station has remained above 20% since 1900 (Evans et al. 2020). The methodology of determining the onset and demise of the rainy season is based on the daily time

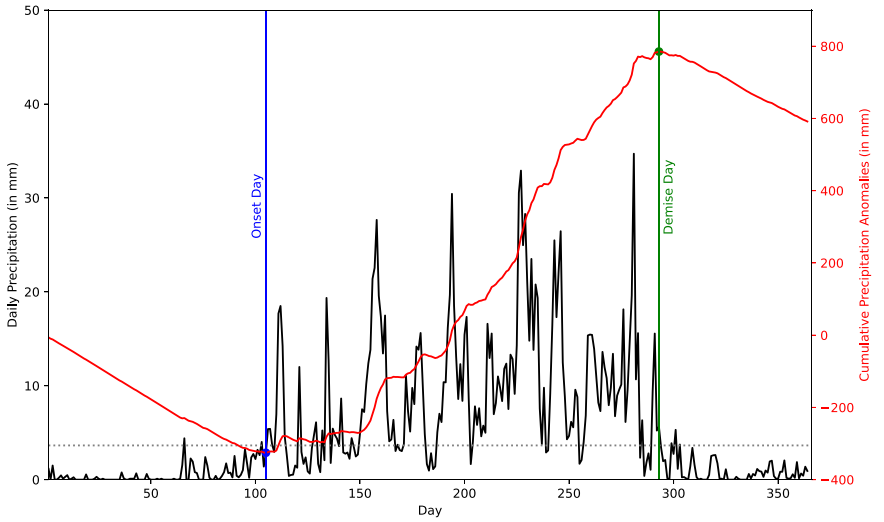

FIG. 2. Illustration of the methodology of the diagnosis of onset and demise of the rainy season for MNW for the year 2000/01, showing the daily time series of rainfall (mm day^{-1}; black line) for the year overlaid with the corresponding daily cumulative anomaly curve (mm; red line). The onset and demise dates are marked on the daily cumulative anomaly curve. The horizontal gray dotted line is the annual mean climatology of the rainfall.

series of precipitation area averaged over the subcluster regions of Australia (weighted by the cosine of the latitude) indicated in Fig. 1. A daily cumulative anomaly curve of precipitation is created for a given subcluster (Fig. 2) from which the minimum and the maximum in the curve are marked as the onset and the demise dates of the rainy season, respectively (e.g., UM20; UM21).

The daily anomalies of the rainfall are obtained by subtracting the annual mean climatology from the daily values of rainfall. This objective criterion of the diagnosis of onset and demise of the rainy season marks the first and the last day of the year in which the daily rainfall is exceeding and receding from the annual mean climatological rainfall, respectively. This methodology has been widely adopted in many other regions, e.g., South America (Liebmann and Marengo 2001), India (Misra and DiNapoli 2014), and Africa (Dunning et al. 2016). Lisonbee et al. (2022) observe false onset of the rainy season over northern Australia, which appears as a period of drought immediately after the onset rains leading to rapid drying of the soil. By definition, and as illustrated in Fig. 2, the diagnosis of the onset and demise of the rainy season is based on the seasonal cycle of the rainfall. The robustness of our methodology stems from the area average of the rainfall over the NRM subclusters that are relatively large, which reduces spurious increases in daily rain rates from isolated rain-bearing systems that may not be part of the seasonal cycle. However, the diagnosis of the onset dates from our methodology does not preclude instances of flash droughts, after onset of the rainy season, as reported in Lisonbee et al. (2022). This will have to be examined in a future study by analyzing the daily distribution of rainfall across the rainy season as defined in this paper for the NRM subclusters, especially in the light of the discovery of trends in short-duration (1–2 day) and long-duration (>3 day) rain events over Australia (Dey et al. 2020).

Given the observational uncertainty in the daily rainfall measurements as delineated in the previous section, we suggest a perturbation of the observed, area-averaged daily precipitation for each of the seven subclusters to produce an ensemble of time series to account for the uncertainty. In addition, the uncertainty of the diagnosis of the onset and demise dates to isolated synoptic and subsynoptic rain-bearing systems also needs to be ascertained. To illustrate this point, take, for example, a null hypothesis that the onset and demise of the rainy season are time invariant and will follow the sinusoidal-like annual cycle, year after year. One way to interpret the perturbations proposed to the time series of the observed daily rainfall here is to find the likelihood of how true or false is such a null hypothesis from the ensemble spread of the diagnosis of the onset and demise dates by perturbing the rainfall at synoptic scales. The perturbations are conducted by randomly perturbing the original time series over a time scale of ±3 days (synoptic scales) to generate 100 perturbed time series. The ensemble mean of 101 such time series of daily rainfall, including the original time series, is shown in Fig. 3 as an illustration of the spread of the time series for MNW.

We also conduct a time-series analysis of the daily, area-averaged rainfall for each subcluster to decompose the temporal variations, using the ensemble empirical mode decomposition (EEMD) following Wu and Huang (2009). This is a data-adaptive methodology that has several advantages over other time-series analysis techniques like the Fourier analysis that, a priori, assume the signal to be described by sine and cosine functions. EEMD isolates the local temporal variations into complete sets of near-orthogonal components called intrinsic mode functions (IMFs). The IMFs can be viewed as basis functions of EEMD that are data adaptive and not predetermined kernels. The IMFs of the EEMD can isolate the Madden–Julian

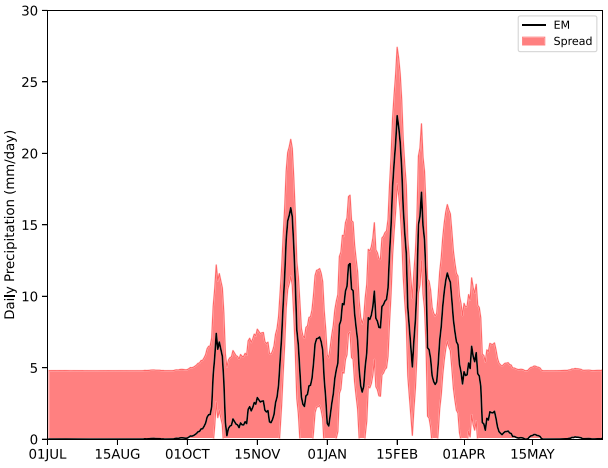

FIG. 3. Daily perturbations of the daily time series of rainfall for MNW for the period 1 Jul 2000–30 Jun 2001. The ensemble mean ("EM") of all the 101 perturbed time series of rainfall is shown in black, and the corresponding 1 standard deviation of daily perturbation ("Spread") is shown in the bounding red shading.

oscillation (MJO) in the 20–70-day time scale from which, over each season, we are able to discern the dry and wet spells from the sign of the anomalies. However, we recognize an MJO event only if the amplitude exceeds 0.5 mm day^{-1} of the filtered MJO time series for each region; otherwise, it is characterized as a weak MJO without identifying its dry or wet spells. The threshold of 0.5 mm day^{-1} was selected to ensure adequate samples of MJOs and yet remove the very-low-amplitude MJOs.

We make use of the observed time series of the mean Niño-3.4 SST index for September–November (SON) and for December–February (DJF), and the SON dipole mode index for the Indian Ocean dipole (IOD), all of which are available from the Physical Sciences Laboratory of NOAA (https://psl.noaa.gov/gcos_wgsp/Timeseries/DMI/; accessed 20 September 2022). These indices are estimated based on the HadISST1.1 SST dataset (Rayner et al. 2003). For both the indices, the 1981–2010 climatology was removed to estimate the monthly anomalies. The filtered tripole index (TPI) for the Interdecadal Pacific Oscillation index (IPO) follows from Henley et al. (2015) (http://psl.noaa.gov/data/timeseries/IPOTPI; accessed 20 September 2022 from). Similarly, the PDO index is based on the leading pattern of EOF of SST anomalies in the North Pacific (Mantua et al. 1997) and was accessed on 20 September 2022 (https://psl.noaa.gov/pdo/). Both these indices are estimated from the Extended Reconstructed SST (ERSST), version 5 (Huang et al. 2017), and the 1981–2010 climatology was removed to estimate the monthly anomalies.

3. Results

a. Onset-date variations

In Fig. 4, we show the variability of the diagnosis of the onset date over the seven subclusters in the form of a box-and-whisker plot. These box-and-whisker plots in Fig. 4 show the median, 25th, and 75th percentiles, and the extreme values that are not outliers (which are defined by values that are greater than 1.5 times the interquartile range) are shown by dots and the outliers by whiskers for the onset date of each rainy season from the ensemble of 101 time series of daily rainfall. From the box-and-whisker plots in Fig. 4, we observe that the ensemble spread of the onset date of the rainy season in the lower latitude regions like MNW, MNE, and wet tropics (WT) is comparatively less relative to the other subclusters. This feature is suggestive of the potential impact of more active (synoptic) weather systems prevailing in the higher latitudes around the start of the rainy season relative to the tropical subclusters. The larger variance in the onset date of the central slopes (CS), ECN, and ECS rainy season in comparison with the tropical clusters in Fig. 4 also suggests that the seasonality of rainfall in the former regions is less robust. This feature manifests with a varied impact on the uncertainty in the diagnosis of the onset dates of the rainy season between the subtropical and tropical NRM subclusters of Australia.

Furthermore, we observe the onset date is strongly correlated with the length of the season and seasonal rainfall anomalies in all the subclusters (Fig. 5). In most regions, except for RLN and MNW, the onset date is insignificantly related to demise-date variations. Figure 5 reveals that early or later onset-date seasons in these subclusters are associated with longer or shorter length of the season and wetter or drier rainy season, respectively. This could be leveraged to provide the rainy season outlook at the beginning of the season from just monitoring of the onset date. A similar approach to provide seasonal outlook by monitoring the onset date of rainy season has been adopted in real time over Florida (Misra et al. 2022).

The long-term trend of earlier onset date as measured by Sen's slope is significant over CS, MNW, and RLN (Fig. 4). At MNW and RLN, the slope of the trend in the onset date occurring earlier at the rate of 0.16 and 0.33 days yr^{-1} is significant at the 99% confidence interval (Fig. 4). In the case of CS, the trend of earlier onset date is 0.23 days yr^{-1}, which is significant at the 90% confidence interval (Fig. 4). In the other regions (ECS, MNE, WT, and MNW), the trends in the onset date of the rainy season are statistically insignificant (Fig. 4).

b. Demise-date variations

The variations of the demise date of the rainy season over these seven subclusters over Australia are shown in Fig. 6. Like Fig. 4, the box-and-whisker plot in Fig. 6 shows the median, interquartile range, extremes, and outliers of the demise date of the rainy season. Once again, we observe that the low-latitude regions of MNW, MNE, and WT show less spread in the demise date than other clusters in comparatively higher latitude regions.

Interestingly, the spread in the demise date (Fig. 6) is higher in all regions relative to the spread in the onset date (Fig. 4). This feature is suggestive of the potential seasonality of the synoptic rainy systems that are more prevalent around the demise date than around the onset date of the rainy season. The correlations in Fig. 5 reveal that the demise-date variations also have a close relationship with the length of the

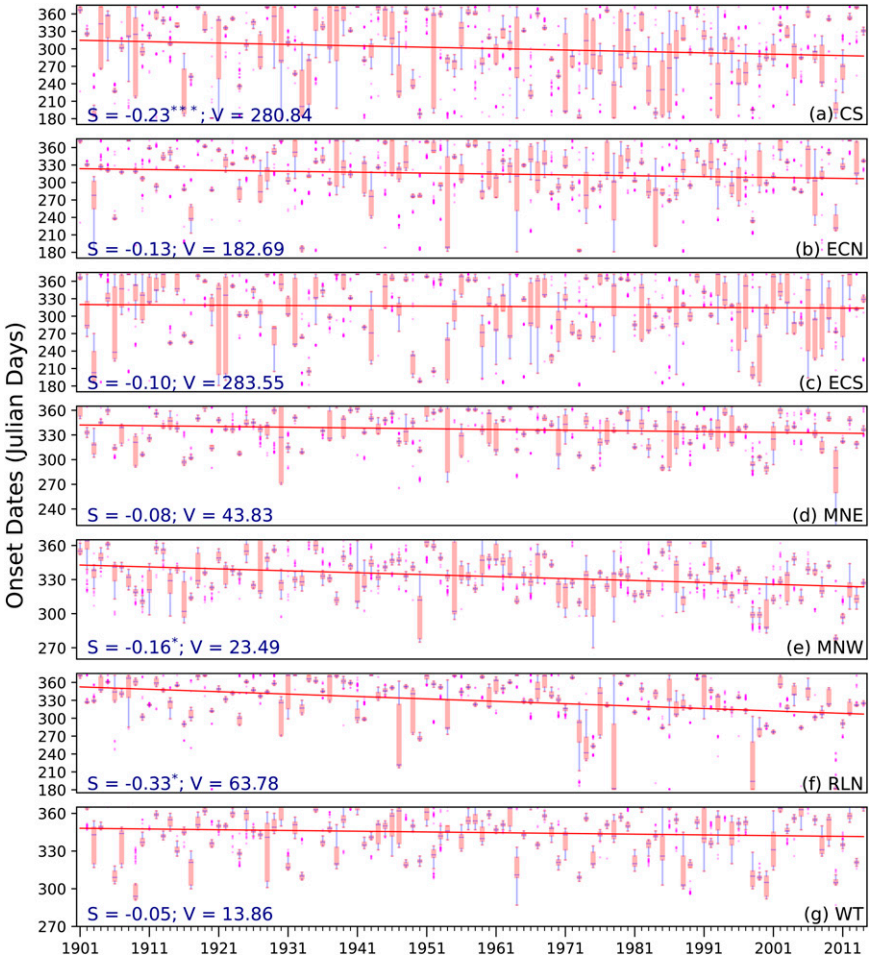

FIG. 4. The box-and-whisker plot (with the boxes indicated by pale red, and the whiskers indicated by blue) of the onset date (yearday) of the rainy season for (a) CS, (b) ECN, (c) ECS, (d) MNE, (e) MNW, (f) RLN, and (g) WT. showing The median values are given by the horizontal line within the boxes, the bottom and top edges of the boxes represent the 25th and the 75th percentiles, whiskers represent the extreme data points of the ensemble spread, and magenta dots represent outliers (which are more than 1.5 times the interquartile range). The red, solid least squares fit line through the median value is overlaid. The variance of the ensemble spread (V; days^2) within the interquartile range is also indicated in the legend. The Sen's slope S (days yr^{-1}) of the trend line is also shown, with three, two, and one asterisk indicating that the slope is significant at the 90%, 95%, and 99% confidence intervals, respectively.

season and the seasonal rainfall anomalies. In all the subclusters, we find that early or late demise of the season is associated with shorter or longer and drier or wetter rainy season, respectively (Fig. 5). The prediction of the variability of demise-date variations of the rainy season is equally important as the onset date, with many impactful applications, like deciding on the last grain harvest of the season (Mollah and Cook 1996) and for the beef sector in northern Australia for planning herd mustering (Chudleigh et al. 2019). However, monitoring of the demise date, unlike the onset date, can only provide a posterior analysis of the evolved rainy season.

The long-term trends in the gradual delay of the demise date of the season over MNW and RLN are 0.13 and 0.28 days yr^{-1}, which are statistically significant at the 95% and 99% confidence intervals, respectively (Fig. 6). The trends of earlier onset and later demise in MNW and RLN also manifest in the corresponding trends of longer (Fig. 7) and wetter (Fig. 8) seasons in MNW and RLN. In other subclusters, the trends of the demise dates are insignificant.

c. *Variations in the length of the season*

It is worthwhile to examine the variations in the length of the season since its variations seem to be related to corresponding variations in onset and demise date in many of the subclusters. In Fig. 7, we show the box-and-whisker plots for the length of the rainy season for the seven subclusters. Yet again, the spread of the length of the season is larger in the higher-latitude regions of RLN, CS, ECS, and ECN relative

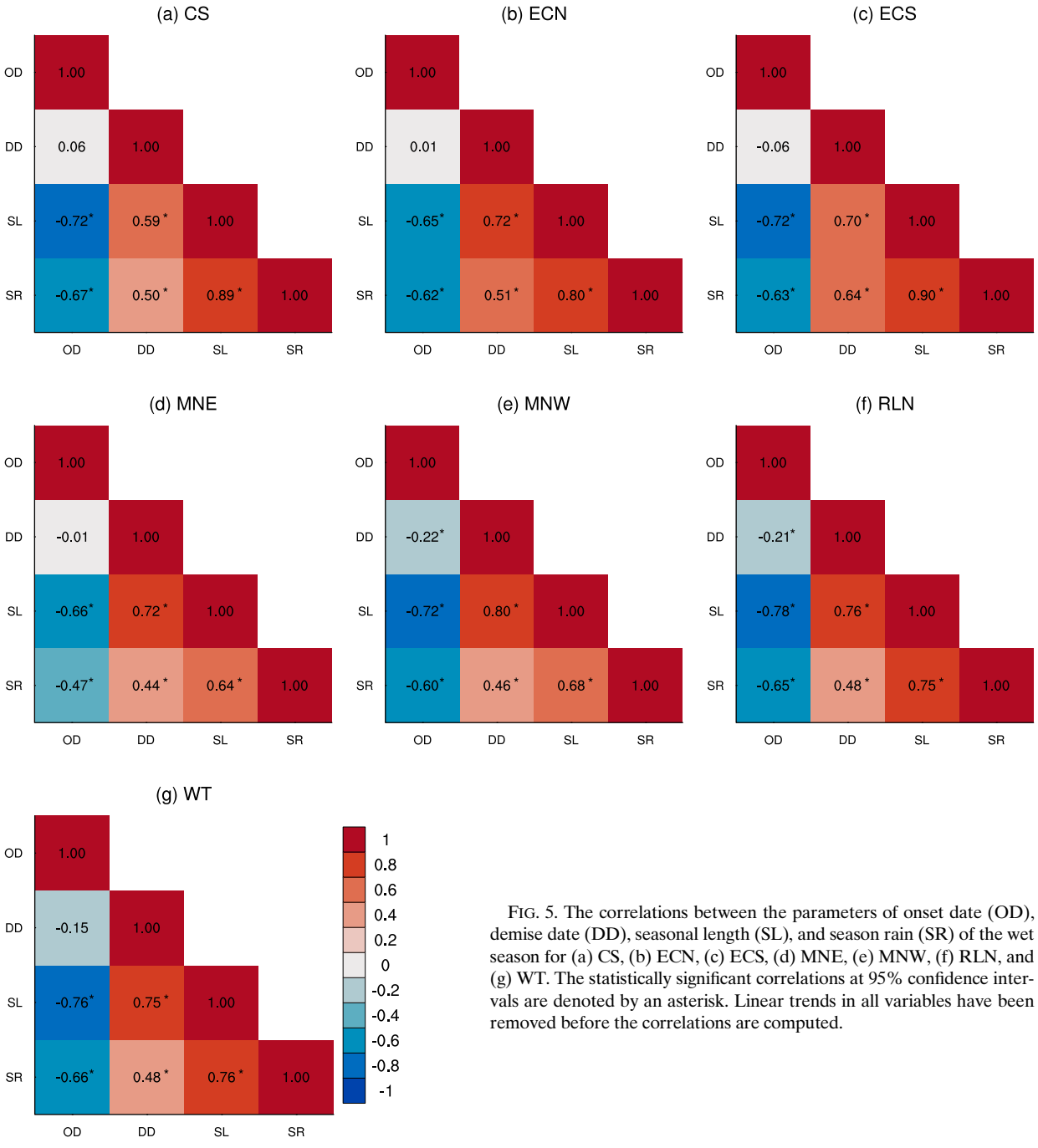

FIG. 5. The correlations between the parameters of onset date (OD), demise date (DD), seasonal length (SL), and season rain (SR) of the wet season for (a) CS, (b) ECN, (c) ECS, (d) MNE, (e) MNW, (f) RLN, and (g) WT. The statistically significant correlations at 95% confidence intervals are denoted by an asterisk. Linear trends in all variables have been removed before the correlations are computed.

to the lower latitude regions of MNE, MNW, and WT (Fig. 7). This is not surprising given that both onset- and demise-date variations displayed a smaller spread in the lower-latitude regions than in the higher-latitude regions. Furthermore, the interquartile spread of the length of the season is larger than the corresponding spread in the demise and the onset dates. Therefore, it can be suggested that predicting the variations in the length of the season could be more challenging than predicting the onset or the demise dates. We find a robust trend of increasing length of the season over MNW and RLN at 0.29 and 0.68 days yr^{-1}, which is significant at the 99% confidence interval (Fig. 7).

Over ECS, the trend of increasing length (at 0.33 days yr^{-1}) of the rainy season is significant at the 90% confidence interval despite insignificant trends in onset and demise date (Fig. 7). This is possible because ECS displays a weak trend toward

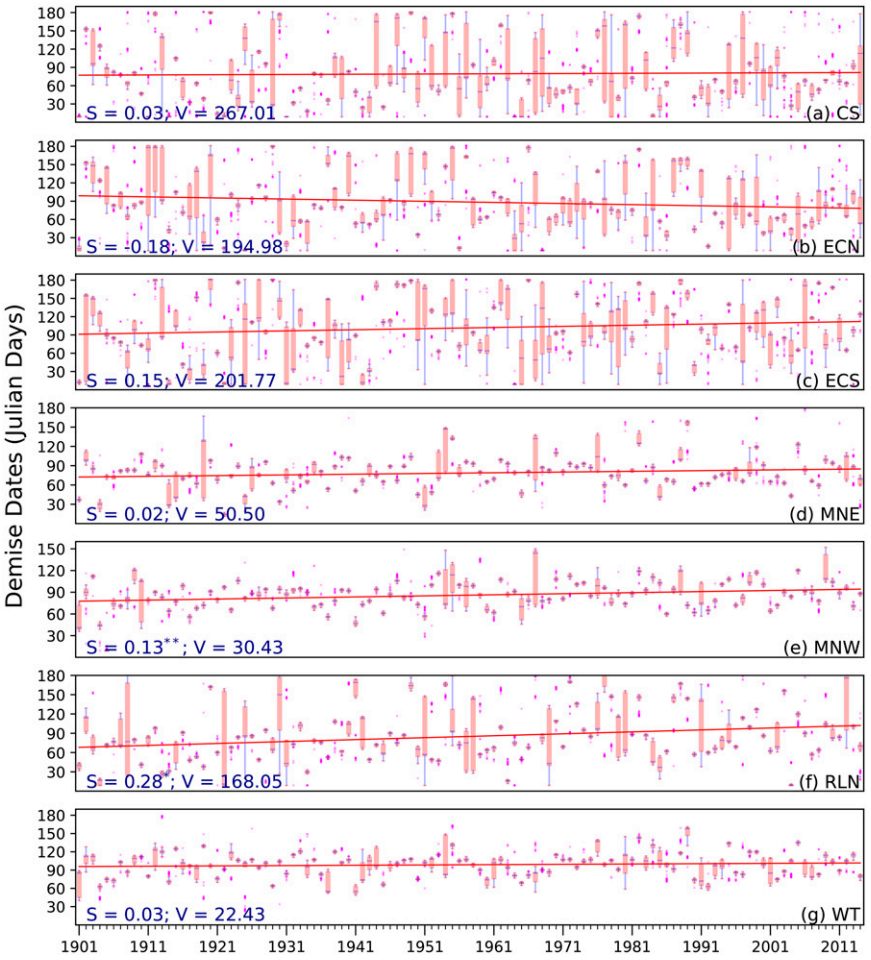

FIG. 6. As in Fig. 4, but for the demise date of the rainy season. For *S*, three, two, and one asterisk indicate that the slope is significant at the 90%, 95%, and 99% confidence intervals, respectively.

earlier onset and later demise dates that ultimately result in the combined influence of lengthening the season. Correspondingly, ECS also displays a trend of a wetter season at 1.64 mm yr^{-1}, significant at the 95% confidence interval (Fig. 8). Similarly, WT and CS show a wetter season trend of 1.6 and 0.9 mm yr^{-1} significant at the 95% and 90% confidence intervals, respectively. In Fig. 8, we also observe that MNW and RNL display significant increasing trends of 3.94 and 1.46 mm yr^{-1} of the seasonal rainfall at the 1% significance level, respectively. This trend is consistent with the corresponding increasing trend of the length of the season from earlier onsets and later demise in the two subclusters. The features of the ensemble spread in the seasonal rain (Fig. 8) are like those of the other variables with subtropical subclusters showing more spread than the tropical subclusters.

d. Intraseasonal variations

U21 noted a robust relationship of the onset- and demise-date variations of the rainy season over northern Australia with the MJO. Similarly, we examined the frequency distribution of the onset date in either of the wet and dry spells of the MJO. We used EEMD to isolate the wet and dry spells of the MJO (Fig. 9a). As noted in U21, the onset date is more frequent during the dry spells over the low-latitude regions of MNW, MNE, and WT. Although, this result seems counterintuitive, U21 found that onset of the rainy season in northern Australia occurs in the last phases of the dry spell of the MJO as it begins to transition to the wet spell of the MJO. We find a similar result in Fig. 9a, with the majority of the onset dates in MNW, MNE, and WT occurring in the dry spells of the MJO. In the subtropical regions of RLN and CS, most of the onset dates occur during the weak MJO period, although in the latter region, wet spells of the MJO also have a significant impact on the onset date of the rainy season (Fig. 9a). However, the conditional distribution of the onset dates to wet, dry, and weak or neutral spells of the MJO for RLN in Fig. 9a is found to be statistically insignificant. Over the eastern coastal regions of ECN and ECS, most of the onset dates occur in the wet spells of the MJO (Fig. 9a).

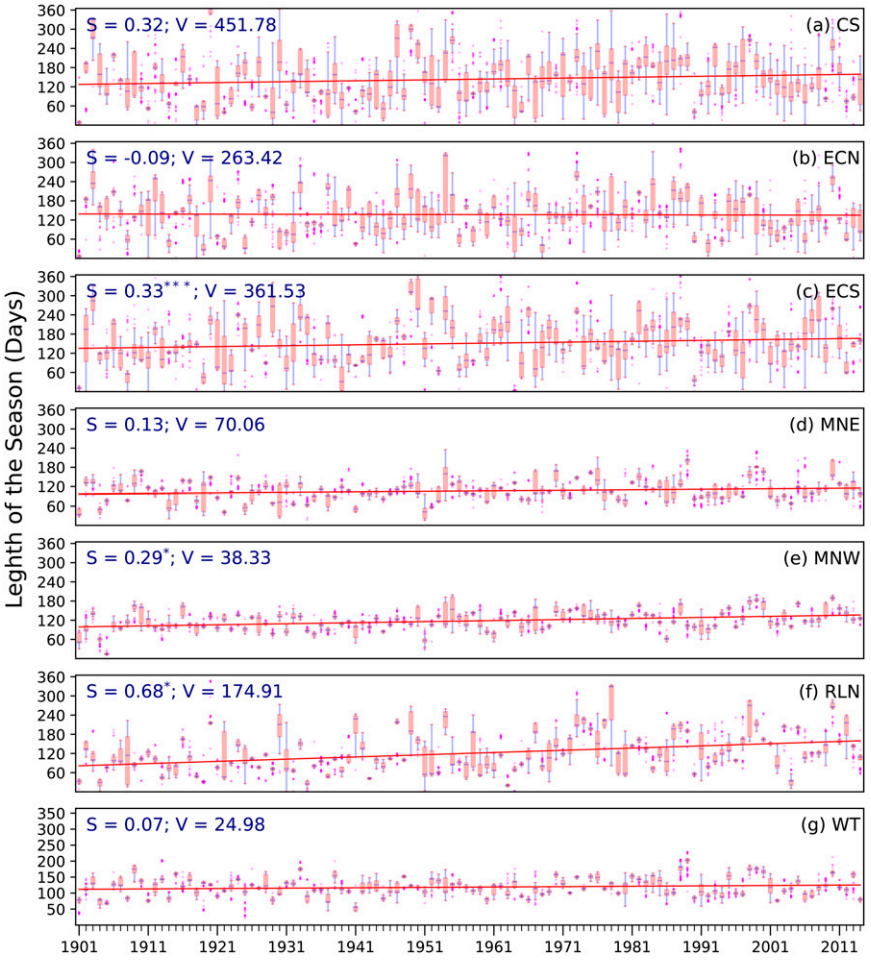

FIG. 7. As in Fig. 6, but for the length (days) of the rainy season.

Unlike the onset-date variations, the MJO phases seem to dictate the variations of the demise date more strongly except over RLN, where the demise date prevails during weak MJO periods (Fig. 9b). With the exception of WT and MNW subclusters, all other regions (besides RLN) exhibit most demise dates in the wet spell period of the MJO. Again, the argument here is that the demise dates mark the transition from the wet to the dry spells of the MJO (U21). The varied influence of MJO on the onset and demise dates of the rainy season in Figs. 9a and 9b potentially suggests the dominance of the seasonal cycle over the MJO in the following manner: Since the demise date marks the day of rain rates decreasing to values below the annual climatological mean for the region, the culmination of the wet spell of MJO with the end of the seasonal cycle of the rainy season will make the large-scale environment far less conducive for sustained and strong atmospheric convection beyond the diagnosed demise date. Therefore, MJO has a strong influence on the demise date. In contrast, even in the absence of a favorable MJO phase, an onset date characterized by rain rates above the annual mean climatological rainfall could be induced by favorable phase of the seasonal cycle. Figure 9 raises the prospect of potentially predicting the onset- and demise-date variations of the rainy season in many of these subclusters at subseasonal scales by leveraging the skills of the MJO prediction in the region.

e. *Interannual variations*

The most robust interannual variability of our climate system is ENSO, which has significant influence on the northern Australian monsoon season (Holland 1986; McBride 1987; Lisonbee et al. 2020). We examine the covariability of the rainy season over these seven subclusters with the seasonal mean SON Niño-3.4 SST index in Fig. 10a. We find that the linear correlation of the ENSO index with the onset date of the rainy season is robust in all seven subclusters, suggesting that early or later onset is likely associated with warm or cold ENSO conditions, respectively.

In contrast, the correlations of the mean SON ENSO index with demise date are much weaker and are only statistically significant in the MNE and MNW regions (Fig. 10a). These correlations remain weak and insignificant even with the use of mean DJF or the mean March–April–May (MAM) Niño-3.4 index (not shown). The correlations of the SON ENSO index with length of the season also shows a robust relationship with

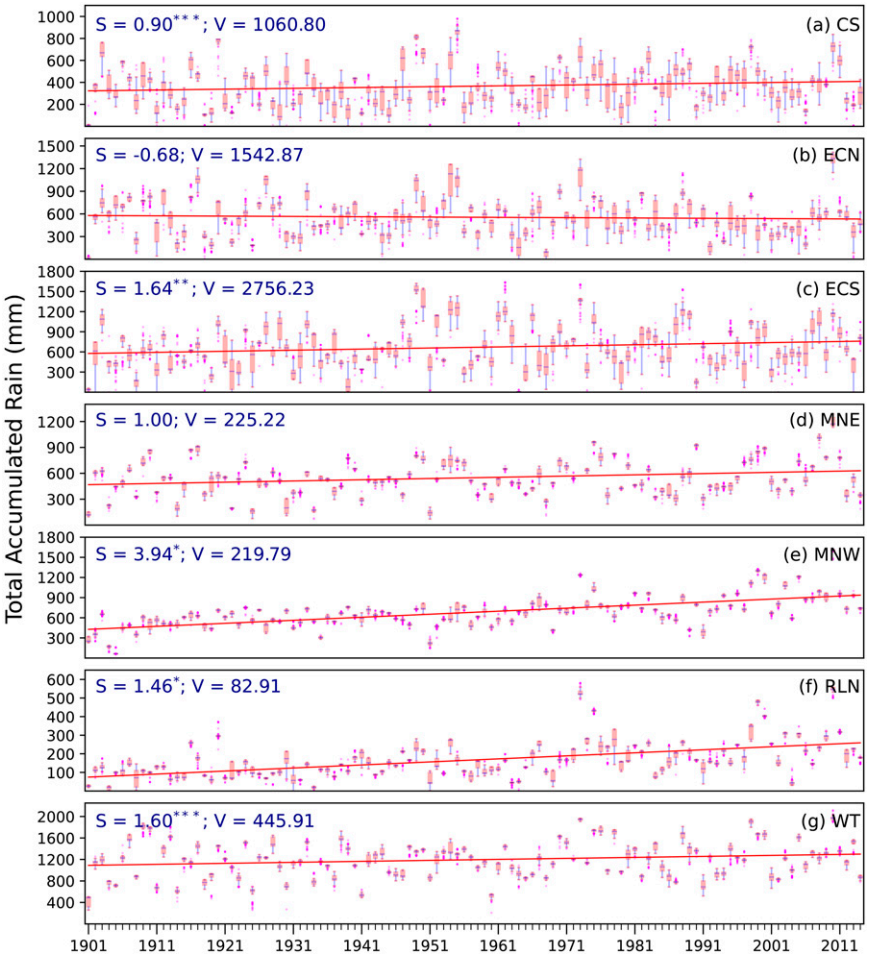

FIG. 8. As in Fig. 6, but for the seasonal rain (mm day^{-1}) of the rainy season; note the units for V [(mm day^{-1})^2] and S (mm day^{-1} yr^{-1}).

warm or cold ENSO events associated with shorter or longer seasons in ECS, MNE, MNW, RLN, and WT (Fig. 10a). Finally, the seasonal rainfall anomaly shows a strong relationship with the SON ENSO index across all seven subclusters with warm or cold ENSO events more likely to be associated with drier or wetter rainy seasons. The dominating influence of the SON ENSO index on the onset date is a result of the peak ENSO variability in SON, while it has less of an influence on the demise date that occurs in February or March, a period when ENSO variability is weakest during the year (Tziperman et al. 1998; Neelin et al. 2000).

In comparison with the ENSO influence, the influence of the IOD on the variations of the rainy season over these subclusters is subtle (Fig. 10b). It may be noted that some studies have pointed to the relatively strong covariation between the ENSO and IOD (Saji et al. 1999; Krishnamurthy and Kirtman 2003). Figure 10b shows that a positive or a negative IOD is likely to be associated with later or earlier onset of the rainy season over WT, MNE, ECN, and CS, which make up the eastern tropical and subtropical parts of Australia. The corresponding influence of IOD on demise date, length of the season, and seasonal rainfall is much weaker (Fig. 10b), given that the annual peak of IOD variations is in the SON season.

f. Decadal variations

The PDO is sometimes claimed as the North Pacific manifestation of the IPO (Heidemann et al. 2022). However, Newman et al. (2016) argue that the IPO is not identical to the PDO. They suggest that the IPO represents a reddened ENSO driven both by interannual and decadal variations of ENSO, while PDO is driven by a multitude of processes, including remote tropical forcing and local North Pacific ocean–atmosphere interactions. Therefore, Newman et al. (2016) claim that the difference between the IPO and PDO is due to chaotic variability internal to North Pacific processes. We examined the relationship of the variability of the rainy season across these seven subclusters in Figs. 11a and 11b with both the IPO and PDO indices.

Figures 11a and 11b suggest overall that the IPO and the PDO have a weaker and a stronger relationship with the rainy seasons across all subclusters, respectively. For example, the onset-date variations in ECS, MNE, MNW, RLN, and WT

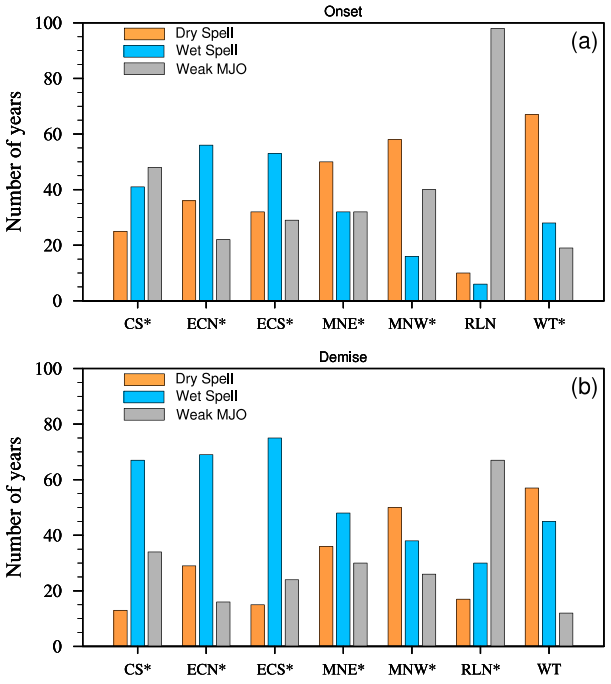

FIG. 9. The frequency of (a) onset and (b) demise dates of the rainy season during the wet (blue) and dry (orange) spells of the MJO and during weak MJO periods (gray) for MNW, WT, MNE, RLN, ECN, CS, and ECS. Asterisks denote that the distribution is significant for the subcluster at the 90% confidence interval according to the bootstrap method.

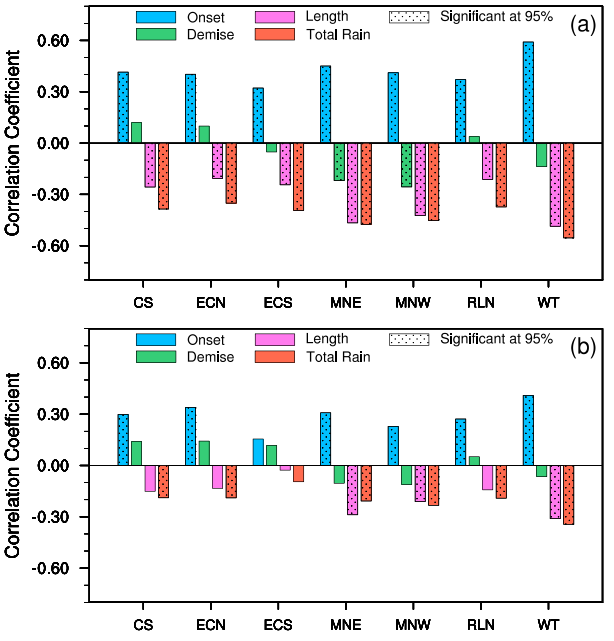

FIG. 10. The correlations of the SON mean (a) Niño-3.4 SST and (b) IOD index with onset and demise dates, length, and seasonal rainfall anomaly of the rainy season over the seven subclusters in Australia. Stippling in the bar indicates that the correlation is significant at the 95% confidence interval according to a *t* test. The correlations are computed after linear trends are removed from all variables.

are significantly modulated by the PDO, with positive PDO associated with later onsets of the rainy season in these regions (Fig. 11b). In contrast, the correlation of the IPO with onset date is weaker and significant only in MNW and RLN (Fig. 11a). Similarly, the demise date, the length of the season, and seasonal rainfall variations are dominated by the PDO with a positive PDO associated with earlier, shorter, and drier rainy season in most of the subclusters. In some of the subclusters like CS, ECN, and ECS, the length and the demise of the season do not exhibit significant correlations with either the IPO (Fig. 11a) or the PDO (Fig. 11b).

4. Discussion

This paper establishes the variability of the rainy season across many of the NRM subclusters associated with the modes of climate variability spanning from the intraseasonal to the secular time scales. This study opens the opportunity to exploit these relationships to explore predictability and useful prediction of the rainy season onset and demise at all these temporal scales. The importance of understanding and predicting the variability of the rainy season in Australia to produce effective management decisions spans across many applied sectors, including but not limited to water and energy production and supply sectors, agriculture, pastoral farming, public health, and wildfire management. It is already encouraging to note that a couple of studies like that of Cowan et al. (2020) and Drosdowsky and Wheeler (2014) have already found useful seasonal predictability skill from operational climate models for the onset date of the wet season (defined as in Lo et al. 2007) over northern Australia. Similar studies could be extended at other time scales and with other definitions of the onset and demise of the rainy season. Sharmila and Hendon (2020), on the other hand, point to local sources of northwestern Australian rainfall variability and predictability from land–atmosphere feedback as opposed to remote teleconnections of ENSO and IPO with northeastern Australian rainfall variations, which can lead to varied predictability of the onset and demise of the rainy season across the continent.

The proposed methodology in this paper could also be exploited for real-time monitoring of the onset date of the rainy season as is currently done over Florida (Misra et al. 2022). The variability of the onset date can provide an outlook of the forthcoming rainy season, with variations of the onset date shown to strongly correlate with the length of the season and the seasonal rainfall anomalies in all the subclusters (Fig. 5).

It is counterintuitive to note in Fig. 11 that the PDO centered in the North Pacific Ocean has stronger relationships to the rainy season over NRM subclusters than the IPO with its SST anomalies centered in the deep tropics, despite several studies suggesting a strong influence of the IPO on Australian rainfall (e.g., Power et al. 1999; Meehl and Arblaster 2011; Heidemann et al. 2022). Heidemann et al. (2022) suggest that IPO–Australian rainfall teleconnection is dominated by the modulation of the Australian monsoon rainfall teleconnection with a specific type of ENSO (the central Pacific type). It is

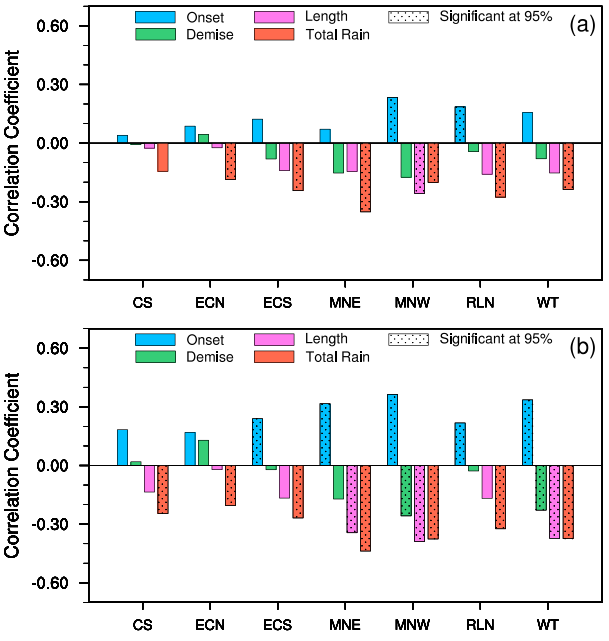

FIG. 11. The correlations of the (a) IPO and the (b) PDO indices with onset and demise dates, length, and seasonal rainfall anomaly of the rainy season over the seven subclusters in Australia. Stippling in the bar indicates that the correlation is significant at the 95% confidence interval according to a *t* test. The correlations are computed after removing the linear trends from all variables.

possible that such diversity in ENSO teleconnections with onset and demise dates of the rainy season of the NRM subclusters may not be as robust and will have to be further investigated. In addition, with spectral peaks of the PDO and IPO ranging between 20 and 70 years, adequate sampling of this variation to establish robust teleconnection is always an issue from contemporary observations. Newman et al. (2016) warn that care should be taken when using the PDO as a forcing function for nonoceanic processes since PDO is largely an oceanic response to atmospheric forcing that spans from tropical to extratropical latitudes.

The robust, increasing trend of seasonal rainfall—lengthening of the rainy season from earlier onset and later demise over RLN and MNW—is consistent with the similar robust, wetter trends observed over the region by Dey et al. (2019a). We have somewhat limited understanding of these trends, given that most contemporary models replicate these historical trends poorly (Dey et al. 2019a,b). Some studies have suggested the role of anthropogenic aerosols that strengthen the monsoonal flow (e.g., Rotstayn et al. 2012; Dey et al. 2019b) and others point to warming of the tropical Atlantic (Lin and Li 2012). There is, however, considerable uncertainty to attribute these trends definitively and this calls for reducing the errors in our climate models.

5. Conclusions

Australia is rich in natural resources. Understanding the climate variations across Australia is critical to manage these resources in a changing climate. In this study, we have examined the observed variability of the rainy season across seven subclusters of Australia that exhibit a strong seasonal cycle in rainfall that is largely coincident with the Australian monsoon season. These subclusters are based on the classification made by the Australian Natural Resource Management agency to develop focused response to climate change. These subclusters range from tropical to subtropical regions and interior to coastal regions. Our analysis reveals that the variability in the evolution of the rainy season manifests distinctly across all temporal scales from the NWP to the secular scales. The higher variability of synoptic weather in the subtropical regions is captured in the contrast of their higher ensemble spread of the onset and demise dates of the rainy season in the subtropical to the lower ensemble spread in the tropical subclusters.

At the intraseasonal scales, we observe that demise-date variations are more strongly modulated than the onset date by the MJO except in RLN, where the MJO has far less influence. The onset and demise dates in many of these subclusters, however, as noted in U21, mark the transition from the dry to wet and wet to dry spells of the MJO, respectively. Similarly, the demise-date variations are more likely associated with the wet spells of the MJO in the CS, ECN, ECS, and MNE subclusters, while over MNW and WT they are more strongly influenced by the dry spells of the MJO. Over the RLN, again, the influence of the MJO on demise-date variations is weak.

At the interannual scales, ENSO variations are a big driver of the variability of the evolution of the rainy season in these clusters. The onset date, length of the rainy season, and seasonal rainfall anomaly across all these seven subclusters are affected by ENSO variations, with warm or cold events likely to be associated with a later or early and drier or wetter season, respectively. The relationship of the ENSO index with demise date is weaker. The relationship of the onset-date variations with length of the season and seasonal rain is also robust and stronger than the corresponding correlations with ENSO index. This provides an opportunity to use the monitoring of the onset date to provide potentially a quick and reliable outlook of the forthcoming season in these subclusters. The demise-date variability, independent of the onset-date variations, has a similar association with the length and seasonal rainfall anomaly of the rainy season. However, the monitoring of the demise date can provide a posterior analysis of the concluded rainy season.

The influence of the IPO and PDO variations with evolution of the rainy season was also investigated across all seven subclusters. The PDO uniformly affects the onset and seasonal rainfall anomaly across all seven subclusters with positive or negative PDO associated with later or early and drier or wetter season, respectively. The IPO, on the other hand, has less uniform impact across the subclusters, with MNW and RLN rainy seasons exhibiting similar teleconnection as with PDO. The secular change or the linear trend is found to be statistically significant in many of the subclusters. There is a statistically significant trend toward an earlier onset and later demise resulting in a longer and wetter season in MNW

and RLN regions. Additionally, WT, CS, and ECS also display a trend toward a wetter rainy season that is coincident with a significant trend of earlier onset in CS and longer season in ECS.

The prediction of the evolution of the rainy season at the higher-latitude subclusters of Australia could be slightly more challenging than the in lower-latitude regions given the larger ensemble spread in the onset and demise of the rainy season regardless of the external influence of the global modes of climate variability. For example, climatology or persistence of onset and demise dates and length of the rainy season are likely to have higher skill in the tropical subclusters of MNE, MNW, and WT relative to other subclusters. Furthermore, the seasonality of the rainfall is weak in some of the subtropical regions like the ECN and ECS (Drosdowsky and Wheeler 2014), which would make variations of the rainy season metrics less applicable in such regions relative to the tropical subclusters. The results of this study are, however, robust given that 114 years of daily rainfall data are used.

Acknowledgments. We acknowledge support from NASA (Grants 80NSSC19K1199 and 80NSSC22K0595).

Data availability statement. The ENSO, DMI, and PDO indices (https://psl.noaa.gov/gcos_wgsp/Timeseries) and the IPO index (https://psl.noaa.gov/data/timeseries/IPOTPI) are available online. The Australian rain gauge analysis is available online (http://www.bom.gov.au/climate/how/newproducts/IDCdrgrids.shtml) for a cost.

REFERENCES

Adam, J. C., and D. P. Lettenmaier, 2003: Adjustment of global gridded precipitation for systematic bias. *J. Geophys. Res.*, **108**, 4257, https://doi.org/10.1029/2002JD002499.

Adams, V. M., J. G. Alvarez-Romeo, S. J. Capon, G. M. Crowley, A. P. Dale, M. J. Kennard, M. M. Douglas, and R. L. Pressey, 2017: Making time for space: The critical role of spatial planning in adapting natural resource management to climate change. *Environ. Sci. Policy*, **74**, 57–67, https://doi.org/10.1016/j.envsci.2017.05.003.

Bardsley, D. K., and G. P. Rogers, 2010: Prioritizing engagement for sustainable adaptation to climate change: An example from natural resource management in South Australia. *Soc. Nat. Resour.*, **24** (1), 1–17, https://doi.org/10.1080/08941920802287163.

Bureau of Meteorology, 2023: Australia's 2021–22 northern wet season. Bureau of Meteorology, accessed 26 January 2023, http://www.bom.gov.au/climate/updates/articles/a041.shtml.

Catto, J. L., N. Nicholls, and C. Jakob, 2012: North Australian sea surface temperatures and the El Niño–Southern Oscillation in observations and models. *J. Climate*, **25**, 5011–5029, https://doi.org/10.1175/JCLI-D-11-00311.1.

Chudleigh, F., T. Oxley, and M. Bowen, 2019: Improving the performance of beef production systems in northern Australia. Queensland government, https://era.daf.qld.gov.au/id/eprint/6153/1/Improving-the-performance-of-beef-production-systems-in-northern-Australia.pdf.

Cowan, T., R. Stone, M. C. Wheeler, and M. Griffiths, 2020: Improving the seasonal prediction of northern Australian rainfall onset to help with grazing management decisions. *Climate Serv.*, **19**, 100182, https://doi.org/10.1016/j.cliser.2020.100182.

Dey, R., S. C. Lewis, J. M. Arblaster, and N. J. Abram, 2019a: A review of past and projected changes in Australia's rainfall. *Wiley Interdiscip. Rev.: Climate Change*, **10**, e577, https://doi.org/10.1002/wcc.577.

——, ——, and N. J. Abram, 2019b: Investigating observed northwest Australian rainfall trends in Coupled Model Intercomparison Project phase 5 detection and attribution experiments. *Int. J. Climatol.*, **39**, 112–127, https://doi.org/10.1002/joc.5788.

——, A. J. E. Gallant, and S. C. Lewis, 2020: Evidence of a continent-wide shift of episodic rainfall in Australia. *Wea. Climate Extremes*, **29**, 100724, https://doi.org/10.1016/j.wace.2020.100274.

Drosdowsky, W., and M. C. Wheeler, 2014: Predicting the onset of the North Australian wet season with the POAMA dynamical prediction system. *Wea. Forecasting*, **29**, 150–161, https://doi.org/10.1175/WAF-D-13-00091.1.

Dunning, C. M., E. C. L. Black, and R. P. Allan, 2016: The onset and cessation of seasonal rainfall over Africa. *J. Geophys. Res. Atmos.*, **121**, 11 405–11 424, https://doi.org/10.1002/2016JD025428.

Ehsani, M. R., and A. Behrangi, 2022: A comparison of correction factors for the systematic gauge-measurement errors to improve the global land precipitation estimate. *J. Hydrol.*, **610**, 127884, https://doi.org/10.1016/j.jhydrol.2022.127884.

Evans, A., D. Jones, R. Smalley, and S. Lellyett, 2020: An enhanced gridded rainfall analysis scheme for Australia. Bureau Research Rep. 041, 39 pp., http://www.bom.gov.au/research/publications/researchreports/BRR-041.pdf.

Evans, S., R. Marchand, and T. Ackerman, 2014: Variability of the Australian monsoon and precipitation trends at Darwin. *J. Climate*, **27**, 8487–8500, https://doi.org/10.1175/JCLI-D-13-00422.1.

Freund, M., B. J. Henley, D. J. Karoly, K. J. Allen, and P. J. Baker, 2017: Multi-century cool and warm season rainfall reconstructions for Australia's major climatic regions. *Climate Past*, **13**, 1751–1770, https://doi.org/10.5194/cp-13-1751-2017.

Grant, I., 2012: Daily rain gauge precipitation (rainfall)–gridded, Australia coverage. Bureau of Meteorology, accessed 21 March 2022, http://data.auscover.org.au/xwiki/bin/view/Product1pages/Product1User1Page1Melbourne12.

Heidemann, H., J. Ribbe, T. Cowan, B. J. Henley, C. Pudmenzky, R. Stone, and D. H. Cobon, 2022: The influence of interannual and decadal Indo-Pacific sea surface temperature variability on Australian monsoon rainfall. *J. Climate*, **35**, 425–444, https://doi.org/10.1175/JCLI-D-21-0264.1.

Hendon, H. H., and B. Liebmann, 1990: The intraseasonal (30–50 day) oscillation of the Australian summer monsoon. *J. Atmos. Sci.*, **47**, 2909–2924, https://doi.org/10.1175/1520-0469(1990)047<2909:TIDOOT>2.0.CO;2.

Henley, B. J., J. Gergis, D. J. Karoly, S. Power, J. Kennedy, and C. K. Folland, 2015: A tripole index for the Interdecadal Pacific Oscillation. *Climate Dyn.*, **45**, 3077–3090, https://doi.org/10.1007/s00382-015-2525-1.

Hennessey, K. J., R. Suppiah, and C. M. Page, 1999: Australian rainfall changes, 1910-1995. *Aust. Meteor. Mag.*, **48**, 1–13.

Holland, G. J., 1986: Interannual variability of the Australian summer monsoon at Darwin: 1952–82. *Mon. Wea. Rev.*, **114**, 594–604, https://doi.org/10.1175/1520-0493(1986)114<0594:IVOTAS>2.0.CO;2.

Huang, B., and Coauthors, 2017: Extended Reconstructed Sea Surface Temperature, version 5 (ERSSTv5): Upgrades, validations, and intercomparisons. *J. Climate*, **30**, 8179–8205, https://doi.org/10.1175/JCLI-D-16-0836.1.

Jones, D. A., W. Wang, and R. Fawcett, 2009: High-quality spatial climate datasets for Australia. *Aust. Meteor. Oceanogr. J.*, **58**, 233–248, https://doi.org/10.22499/2.5804.003.

Kajikawa, Y., B. Wang, and J. Yang, 2010: A multi-time scale Australian monsoon index. *Int. J. Climatol.*, **30**, 1114–1120, https://doi.org/10.1002/joc.1955.

King, A. D., L. V. Alexander, and M. G. Donat, 2013: The efficacy of using gridded data to examine extreme rainfall characteristics: A case study for Australia. *Int. J. Climatol.*, **33**, 2376–2387, https://doi.org/10.1002/joc.3588.

Krishnamurthy, V., and B. P. Kirtman, 2003: Variability of the Indian Ocean: Relation to monsoon and ENSO. *Quart. J. Roy. Meteor. Soc.*, **129**, 1623–1646, https://doi.org/10.1256/qj.01.166.

Liebmann, B., and J. Marengo, 2001: Interannual variability of the rainy season and rainfall in the Brazilian Amazon basin. *J. Climate*, **14**, 4308–4318, https://doi.org/10.1175/1520-0442(2001)014<4308:IVOTRS>2.0.CO;2.

Lin, Z., and Y. Li, 2012: Remote influence of the tropical Atlantic on the variability and trend in North West Australia summer rainfall. *J. Climate*, **25**, 2408–2420, https://doi.org/10.1175/JCLI-D-11-00020.1.

Lisonbee, J., J. Ribbe, and M. Wheeler, 2020: Defining the north Australian monsoon onset: A systematic review. *Prog. Phys. Geogr.*, **44**, 398–418, https://doi.org/10.1177/0309133319881107.

——, ——, J. A. Otkin, and C. Pudmenzky, 2022: Wet season rainfall onset and flash drought: The case of the northern Australian wet season. *Int. J. Climatol.*, **42**, 6499–6514, https://doi.org/10.1002/joc.7609.

Lo, F., M. C. Wheeler, H. Meinke, and A. Donald, 2007: Probabilistic forecasts of the onset of the north Australian wet season. *Mon. Wea. Rev.*, **135**, 3506–3520, https://doi.org/10.1175/MWR3473.1.

Mantua, N. J., S. R. Hare, Y. Zhang, J. M. Wallace, and R. C. Francis, 1997: A Pacific interdecadal climate oscillation with impacts on salmon production. *Bull. Amer. Meteor. Soc.*, **78**, 1069–1080, https://doi.org/10.1175/1520-0477(1997)078<1069:APICOW>2.0.CO;2.

McBride, J. L., 1987: The Australian summer monsoon. *Reviews of Monsoon Meteorology*, C. P. Chang and T. N. Krishnamurti, Eds., Oxford University Press, 203–231.

——, and N. Nicholls, 1983: Seasonal relationships between Australian rainfall and the Southern Oscillation. *Mon. Wea. Rev.*, **111**, 1998–2004, https://doi.org/10.1175/1520-0493(1983)111<1998:SRBARA>2.0.CO;2.

Meehl, G. A., and J. M. Arblaster, 2011: Decadal variability of Asian–Australian monsoon–ENSO–TBO relationships. *J. Climate*, **24**, 4925–4940, https://doi.org/10.1175/2011JCLI4015.1.

Misra, V., and S. DiNapoli, 2014: The variability of the Southeast Asian summer monsoon. *Int. J. Climatol.*, **34**, 893–901, https://doi.org/10.1002/joc.3735.

——, C. B. Jayasankar, P. Beasley, and A. Bhardwaj, 2022: Operational monitoring of the evolution of the rainy season over Florida. *Front. Climate*, **4**, 793959, https://doi.org/10.3389/fclim.2022.793959.

Mollah, W. W., and I. M. Cook, 1996: Rainfall variability and agriculture in the semi-arid tropics–the Northern Territory, Australia. *Agric. For. Meteor.*, **79**, 39–60, https://doi.org/10.1016/0168-1923(95)02267-8.

Neelin, J. D., F.-F. Jin, and H.-H. Syu, 2000: Variations in ENSO phase locking. *J. Climate*, **13**, 2570–2590, https://doi.org/10.1175/1520-0442(2000)013<2570:VIEPL>2.0.CO;2.

Newman, M., and Coauthors, 2016: The Pacific decadal oscillation, revisited. *J. Climate*, **29**, 4399–4427, https://doi.org/10.1175/JCLI-D-15-0508.1.

Nicholls, N., 1984: A system for predicting the onset of the north Australian wet season. *J. Climatol.*, **4**, 425–435, https://doi.org/10.1002/joc.3370040407.

——, J. L. McBride, and R. J. Ormerod, 1982: On predicting the onset of the Australian wet season at Darwin. *Mon. Wea. Rev.*, **110**, 14–17, https://doi.org/10.1175/1520-0493(1982)110<0014:OPTOOT>2.0.CO;2.

Power, S., T. Casey, C. Folland, A. Colman, and V. Mehta, 1999: Inter-decadal modulation of the impact of ENSO on Australia. *Climate Dyn.*, **15**, 319–324, https://doi.org/10.1007/s003820050284.

Rayner, N. A., D. E. Parker, E. B. Horton, C. K. Folland, L. V. Alexander, D. P. Rowell, E. C. Kent, and A. Kaplan, 2003: Global analyses of sea surface temperature, sea ice, and night marine air temperature since the late nineteenth century. *J. Geophys. Res.*, **108**, 4407, https://doi.org/10.1029/2002JD002670.

Rotstayn, L. D., S. J. Jeffrey, M. A. Collier, S. M. Dravitzki, A. C. Hirst, J. I. Syktus, and K. K. Wong, 2012: Aerosol- and greenhouse gas-induced changes in summer rainfall and circulation in the Australasian region: A study using single-forcing climate simulations. *Atmos. Chem. Phys.*, **12**, 6377–6404, https://doi.org/10.5194/acp-12-6377-2012.

Saji, N. H., B. N. Goswami, P. N. Vinayachandran, and T. Yamagata, 1999: A dipole mode in the tropical Indian Ocean. *Nature*, **401**, 360–363, https://doi.org/10.1038/43854.

Schneider, U., A. Becker, P. Finger, A. Meyer-Christoffer, M. Ziese, and B. Rudolf, 2014: GPCC's new land surface precipitation climatology based on quality-controlled in situ data and its role in quantifying the global water cycle. *Theor. Appl. Climatol.*, **115**, 15–40, https://doi.org/10.1007/s00704-013-0860-x.

Sevruk, B., M. Ondras, and B. Chvila, 2009: The WMO precipitation measurement intercomparisons. *Atmos. Res.*, **92**, 376–380, https://doi.org/10.1016/j.atmosres.2009.01.016.

Sharmila, S., and H. H. Hendon, 2020: Mechanisms of multiyear variations of northern Australia wet-season rainfall. *Sci. Rep.*, **10**, 5086, https://doi.org/10.1038/s41598-020-61482-5.

Taschetto, A. S., and M. H. England, 2009: An analysis of late twentieth century trends in Australian rainfall. *Int. J. Climatol.*, **29**, 791–807, https://doi.org/10.1002/joc.1736.

Troup, A. J., 1961: Variations in upper tropospheric flow associated with the onset of the Australian monsoon. *Indian J. Meteor. Geophys.*, **12**, 217–230, https://doi.org/10.54302/mausam.v12i2.4184.

Tziperman, E., M. A. Cane, S. E. Zebiak, Y. Xue, and B. Blumenthal, 1998: Locking of El Niño's peak time to the end of the calendar year in the delayed oscillator picture of ENSO. *J. Climate*, **11**, 2191–2199, https://doi.org/10.1175/1520-0442(1998)011<2191:LOENOS>2.0.CO;2.

Uehling, J., and V. Misra, 2020: Characterizing the seasonal cycle of the northern Australian rainy season. *J. Climate*, **33**, 8957–8973, https://doi.org/10.1175/JCLI-D-19-0592.1.

——, ——, A. Bhardwaj, and N. Karmakar, 2021: Characterizing the local variations of the northern Australian rainy season. *Mon. Wea. Rev.*, **149**, 3995–4004, https://doi.org/10.1175/MWR-D-21-0093.1.

Wu, Z., and N. E. Huang, 2009: Ensemble empirical mode decomposition: A noise-assisted data analysis method. *Adv. Adapt. Data Anal.*, **1**, 1–41, https://doi.org/10.1142/S1793536909000047.